Supporting Information for "Multiple large-scale dynamical pathways for pan–Atlantic compound cold and windy extremes"

Jacopo Riboldi[1], Richard Leeding[1], Antonio Segalini[1], Gabriele Messori[1,2,3]

[1]Department of Earth Sciences, Uppsala University, Uppsala, Sweden

[2]Centre of natural Hazards and Disaster Science (CNDS), Uppsala University, Uppsala, Sweden

[3]Department of Meteorology and Bolin Centre for Climate Research, Stockholm University, Stockholm, Sweden

Contents of this file

1. Text S1

2. Figures S1 to S4

3. Tables S1

Introduction

This Supporting Information contains:

- a detailed description of the computation and the filtering of wave activity flux;

- four supplementary figures that integrate the results exposed in the paper;

- a table with the list of analyzed North American cold spells.

December 12, 2022, 4:54pm

Text S1. Notes about wave-activity flux computation and filtering The computation of the wave-activity flux is based on ERA5 geopotential and wind data, using a NCAR Command Language (NCL) script developed by Kazuaki Nishii, publicly available at http://www.atmos.rcast.u-tokyo.ac.jp/nishii/programs/index.html. It is based on anomalies of geostrophic streamfunction at $250\,\mathrm{hPa}$

$$\psi' = \Phi'_{250}/f \tag{1}$$

where Φ'_{250} is the geopotential ($\Phi = gz$) anomaly at the same level and f is the latitude-dependent Coriolis parameter. Anomalies are obtained with respect to the seasonal cycle, calculated from the 30-day-running mean of geopotential for each calendar day. The two horizontal components of the wave activity flux $\mathbf{WAF} = (\mathrm{WAF}_x, \mathrm{WAF}_y)$ are then defined as

$$\mathrm{WAF}_x = \frac{p}{1000}\frac{1}{2|\mathbf{U}|a^2}\left\{\frac{U}{\cos\phi}\left[\left(\frac{\partial\psi'}{\partial\lambda}\right)^2 - \psi'\frac{\partial^2\psi'}{\partial\lambda^2}\right] + V\left[\frac{\partial\psi'}{\partial\lambda}\frac{\partial\psi'}{\partial\phi} - \psi'\frac{\partial^2\psi'}{\partial\psi\partial\phi}\right]\right\} \tag{2}$$

$$\mathrm{WAF}_y = \frac{p}{1000}\frac{1}{2|\mathbf{U}|a^2}\left\{\left[U\frac{\partial\psi'}{\partial\lambda}\frac{\partial\psi'}{\partial\phi} - \psi'\frac{\partial^2\psi'}{\partial\psi'\partial\phi}\right] + V\cos\phi\left[\left(\frac{\partial\psi'}{\partial\phi}\right)^2 - \psi'\frac{\partial^2\psi'}{\partial\phi^2}\right]\right\} \tag{3}$$

where λ is the longitude, ϕ is the latitude and $|\mathbf{U}| = (U, V)$ is the background climatology of the zonal and meridional component of the wind at $250\,\mathrm{hPa}$, also obtained from the 30-day-smoothed seasonal cycle. As we are considering only the slow-moving, low-frequency flow component, we neglect here the additional term corresponding to the phase propagation of the wave in the direction of the background wind (present instead in the formulation of Takaya & Nakamura, 2001).

Given that the $\mathbf{WAF}$ field resulting from the computation featured variations at a very small scale (which is inconsistent with the applied low-pass time filtering, as noticed by

Wolf & Wirth, 2017), a truncation based on spherical harmonics was further applied to eliminate numerical noise. This filter exploited the spatial coherence of planetary-scale motions providing a sufficiently smooth spatial field at every instant. The **WAF** field at a given pressure level was first projected in a space spanned by spherical harmonics, $Y_n^m(\phi, \lambda)$, by means of the Python routine shtns (Schaeffer, 2013). The filtering is then performed by suppressing all the components with degree $n > 20$, corresponding to eliminating all variations with wavenumber larger than 20 in both the zonal and meridional direction. The filtered spatial field was constructed by inverting the modified spherical harmonics projection. Figure S1 shows an example of the resulting filtered field from a WAF_x spatial field where it can be clearly observed that the filter keeps the large coherent features and removes the fine-grained noise, facilitating the assessment of the wave activity flux.

References

Schaeffer, N. (2013). Efficient spherical harmonic transforms aimed at pseudospectral numerical simulations. *Geochemistry, Geophysics, Geosystems*, *14*(3), 751–758.

Takaya, K., & Nakamura, H. (2001). A formulation of a phase-independent wave-activity flux for stationary and migratory quasigeostrophic eddies on a zonally varying basic flow. *J. Atmos. Sci.*, *58*, 608 - 627. doi: 10.1175/1520-0469(2001)058⟨0608:AFOAPI⟩2.0.CO;2

Wolf, G., & Wirth, V. (2017). Diagnosing the horizontal propagation of Rossby wave packets along the midlatitude waveguide. *Mon. Wea. Rev.*, *145*, 3247–3264. doi: 10.1175/MWR-D-16-0355.1
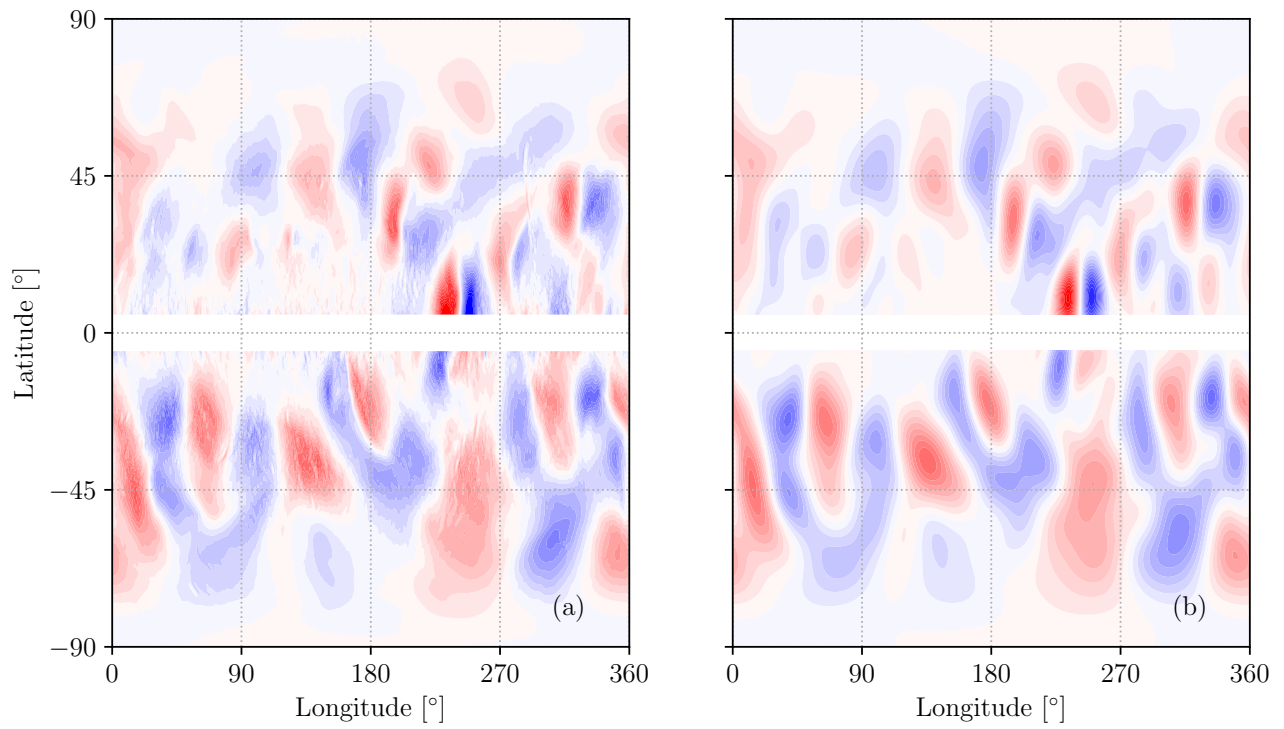
Figure S1. Comparison between (a) the WAF$_x$ field for the 24. Dec. 1979 and (b) its filtered version.
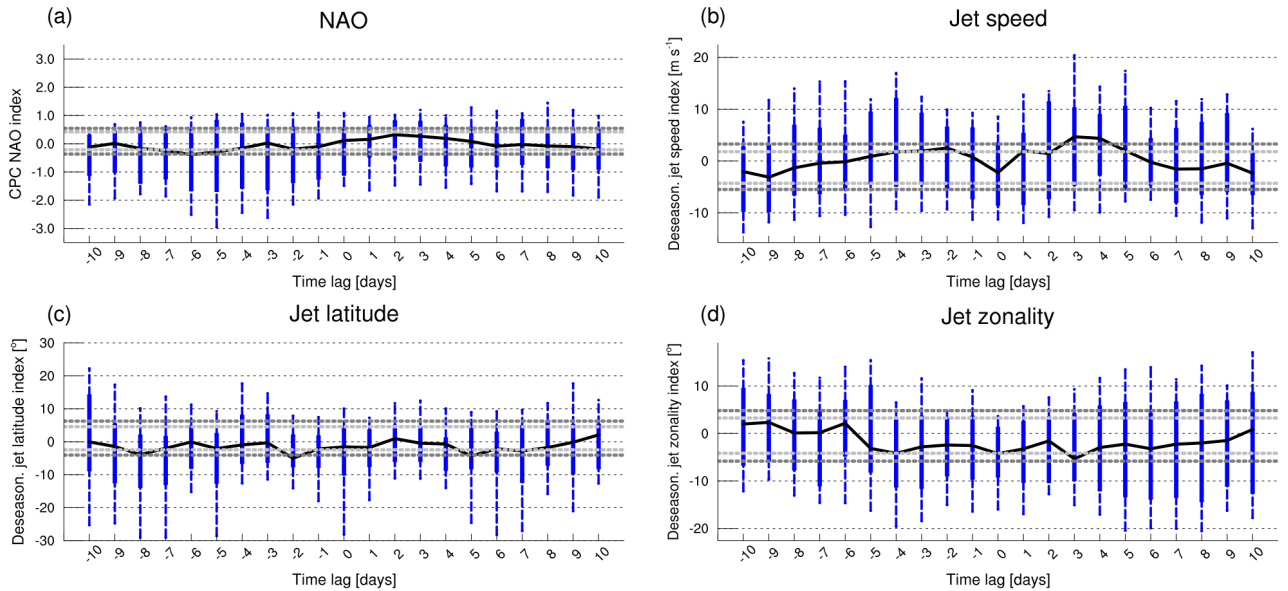
Figure S2. Distributions of (a) North Atlantic Oscillation (NAO), (b) jet speed (c) jet latitude and (d) jet zonality indices for the considered 35 Central NA cold spells (in blue). The lower (upper) whisker marks the lower (upper) decile of each distribution. The black bold line connects the medians at each time step, while the lower (upper) bound of the box indicates the lower (upper) quartile. The dark (light) grey dotted lines refer to the top/bottom 1% (5%) of a 10.000-times randomly resampled distribution of the same quantity.
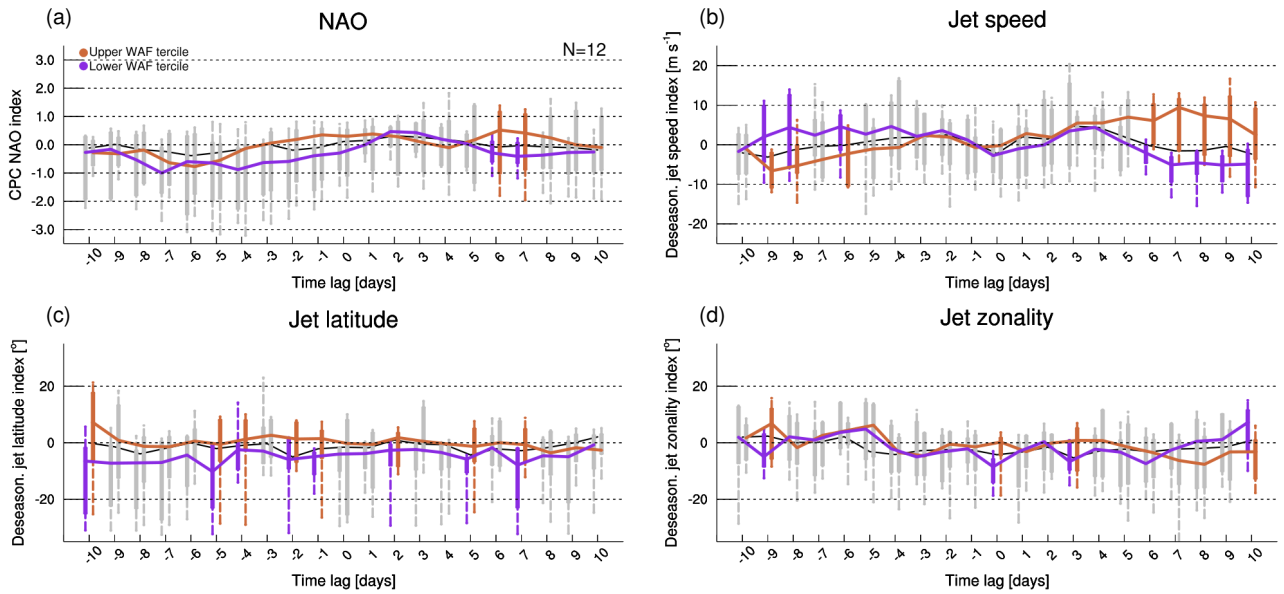
**Figure S3.**   Distributions of (a) North Atlantic Oscillation (NAO), (b) jet speed (c) jet latitude and (d) jet zonality indices for the 12 Central NA cold spells in the WAF+ (orange) and WAF- (indigo) subsets. Only time lags with a difference between the subset medians in the top/bottom 5% of a 10.000-times random reshuffling of the two subsets are colored. Box-and-whiskers diagrams as in Fig. S2.
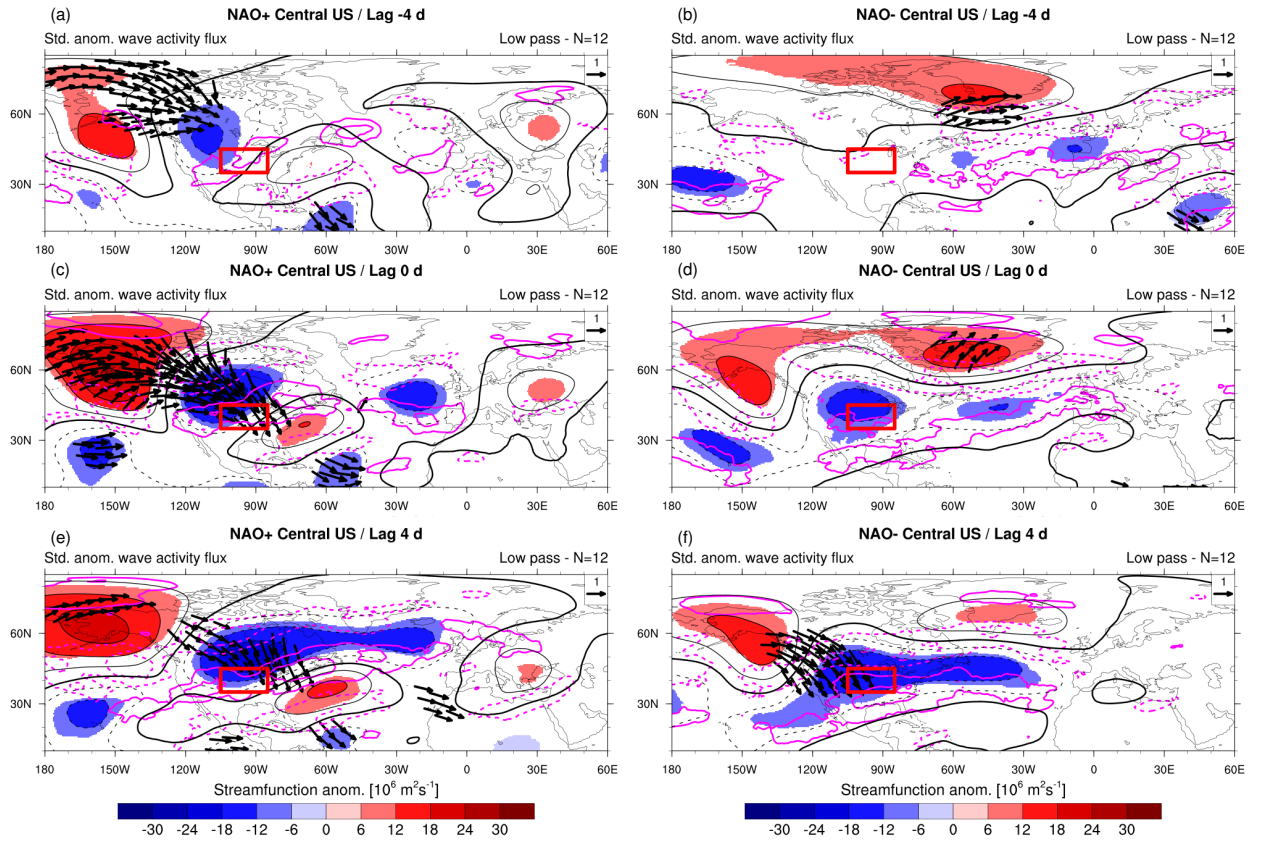
Figure S4. Lagged composited of standardized WAF anomalies (arrows), geostrophic stream-function anomalies (shaded) and $250\,\mathrm{hPa}$ zonal wind anomalies (magenta contours, only $\pm 5\,\mathrm{m\,s^{-1}}$, $\pm 10\,\mathrm{m\,s^{-1}}$, negative values dashed) for the 12 central NA cold spells in the (left) NAO+ and (right) NAO- subsets at lags (a,d) t_{CS}-4 d (b,e) t_{CS}, and (c,f) t_{CS}+4 d. Only significant WAF vectors and streamfunction anomalies are shown (with respect to the top 99% or bottom 1% of a bootstrapped distribution).

Table S1.   List of 35 cold spells in the Central North America region considered in this study, ordered with respect to the area-averaged wave activity flux (WAF) in the region. Cold spells belonging to the upper (WAF+) and lower (WAF-) tercile subsets are indicated in the last column.

Number	Date	WAF $[10^6\,\mathrm{m}^2\,\mathrm{s}^{-2}]$	Subset
1	1985-02-02	142.67	WAF+
2	2013-12-08	82.61	WAF+
3	1990-12-24	61.80	WAF+
4	1989-02-05	53.30	WAF+
5	1994-01-17	33.96	WAF+
6	2006-02-19	33.68	WAF+
7	2010-01-07	32.24	WAF+
8	1982-02-08	29.39	WAF+
9	1983-12-24	26.16	WAF+
10	2018-01-01	24.57	WAF+
11	1993-02-18	22.57	WAF+
12	1980-01-29	22.31	WAF+
13	2008-01-22	22.28	
14	2006-12-02	19.31	
15	2003-01-24	19.28	
16	2005-12-07	19.01	
17	1984-01-19	18.85	
18	2009-01-26	18.30	
19	1983-12-01	17.75	
20	2015-02-21	17.37	
21	2009-12-09	16.51	
22	1991-12-03	15.93	
23	2011-02-09	15.89	
24	1982-01-11	15.83	WAF-
25	1981-02-11	12.97	WAF-
26	2014-02-08	12.45	WAF-
27	2000-12-13	12.35	WAF-
28	1989-12-21	12.11	WAF-
29	1997-01-12	10.64	WAF-
30	2003-02-25	9.87	WAF-
31	1985-12-01	8.46	WAF-
32	1986-02-11	7.45	WAF-
33	2007-02-15	7.03	WAF-
34	1988-01-07	5.99	WAF-
35	1996-02-02	5.28	WAF-